

INTRINSIC AND EXTRINSIC SIZE EFFECTS IN MATERIALS

Hexagonal close-packed high-entropy alloy formation under extreme processing conditions

Ram Devanathan^{1,a)} , Weilin Jiang¹, Karen Kruska¹, Michele A. Conroy^{1,b)}, Timothy C. Droubay², Jon M. Schwantes³

¹Energy and Environment Directorate, Pacific Northwest National Laboratory, Richland, Washington 99352, USA

²Physical and Computational Sciences Directorate, Pacific Northwest National Laboratory, Richland, Washington 99352, USA

³National Security Directorate, Pacific Northwest National Laboratory, Richland, Washington 99352, USA

^{a)}Address all correspondence to this author. e-mail: ram.devanathan@pnnl.gov

^{b)}This work was performed while M.A. Conroy was at Pacific Northwest National Laboratory.

Received: 7 September 2018; accepted: 29 October 2018

We assess the validity of criteria based on size mismatch and thermodynamics in predicting the stability of the rare class of high-entropy alloys (HEAs) that form in the hexagonal close-packed crystal structure. We focus on nanocrystalline HEA particles composed predominantly of Mo, Tc, Ru, Rh, and Pd along with Ag, Cd, and Te, which are produced in uranium dioxide fuel under the extreme conditions of nuclear reactor operation. The constituent elements are fission products that aggregate under the combined effects of irradiation and elevated temperature as high as 1200 °C. We present the recent results on alloy nanoparticle formation in irradiated ceria, which was selected as a surrogate for uranium dioxide, to show that radiation-enhanced diffusion plays an important role in the process. This work sheds light on the initial stages of alloy nanoparticle formation from a uniform dispersion of individual metals. The remarkable chemical durability of such multiple principal element alloys presents a solution, namely, an alloy waste form, to the challenge of immobilizing Tc.

Introduction

High-entropy alloys (HEAs), which are composed of five or more metals in near-equiatomic proportions [1], have attracted growing attention due to fundamental scientific interest in phase stability and promising structural applications. While initial work focused on entropic stabilization of disordered solid solutions, it is now recognized that contributions other than configurational entropy must be considered to understand and predict the occurrence of single-phase solutions [3, 4, 5, 6, 7, 8, 9, 10, 11]. Configurational entropy is sensitive to short-range order that varies with temperature. Vibrational entropy also contributes to total entropy. This contribution can be predicted from density functional theory (DFT) [12] and hybrid Monte Carlo/molecular dynamics simulations, which were reviewed in a recent paper [13]. This finding has given rise to terms such as multi-principal element alloys (MPEAs) [14] or complex concentrated alloys [15] to describe alloys that are located away from the edges and vertices of multicomponent phase diagrams (ternary and higher). The common feature of these definitions is the alloying strategy using multiple major

elements instead of the conventional vertex-and-edge approach of starting with a dominant base metal and adding one or more alloying elements. Most of the interest in these alloys is driven by structural properties [1, 16, 17, 18, 19], although precious metal HEAs have particular applications in catalysis [20]. The present work is motivated by an unusual application of HEAs—the immobilization of high-level nuclear waste.

Recently, Miracle and Senkov [6] performed a thorough assessment of the relatively unexplored central region of the multicomponent alloy phase diagram space. Of the 408 published alloys studied by these authors, 85% contained at least four of the following elements: Al, Co, Cr, Cu, Fe, Mn, Ni, Ti, and V. About 81% of the alloys studied contained Fe. These compositions can be considered extensions of widely studied austenitic stainless steels, austenitic Ni-based alloys, and Ni-based superalloys. Solid solutions constituted 48% of the reported microstructures, with single-phase solid solutions occurring in only 25% of the microstructures. The face-centered cubic (FCC), body-centered cubic (BCC), and hexagonal close-packed (HCP) phases occurred in the ratio



56:43:1. This proportion does not consider intermetallic compounds that are commonly found in HEAs. HCP phases and single-phase HCP solid solutions that are the subjects of this report are rare among HEAs [21]. It is worth noting that experimental results show a stronger preference for solid solutions and single-phase microstructures compared to CALPHAD results. The CALPHAD also overestimates the occurrence of HCP phases [6]. These discrepancies stem from a number of reasons. Experimental microstructure reports by different groups for the same alloy differ because of differences in processing conditions. The reported microstructures may not be at equilibrium. Thermomechanical treatments following synthesis can cause new phases to form. Thermodynamics databases have limited data for most HEAs. The energetics of HCP phases are nearly the same as those of FCC phases due to similar arrangement of first neighbor atoms. Widom [7] has recently reviewed in detail the key issues in modeling the structure and thermodynamics of HEAs.

Hexagonal HEAs

Several groups have pursued the synthesis of HCP HEAs considering their rarity. Zhang et al. [8] have pointed out the lack of reports on HCP HEAs but stated that the HCP phase can form in HEAs composed of rare earth elements with the HCP structure if they have similar atomic radii and form isomorphous binary solid solutions. Feuerbacher et al. [22] have synthesized an HCP alloy composed of YGdTbDyHo in equiatomic proportions by melting the pure elements in an Ar atmosphere and remelting the ingot four times for homogenization. The samples were homogenous and single phase with space group $P6_3/mmc$. The lattice constants were $a = 0.363$ nm and $c = 0.566$ nm. Based on thermodynamic considerations, atomic radii, and high mutual solubility in binary solutions, Feuerbacher et al. [22] have stated that hexagonal HEAs can be formed by including La, Er, Tm, Lu, Pr, Pm, and Nd. Other hexagonal HEA compositions have been predicted by calculations [23] but may be challenging to synthesize due to the drastic differences in melting points of constituents, such as Co and Re [22].

Takeuchi et al. [24] have designed HCP HEAs by considering crystal structure and thermodynamic data from binary phase diagrams. They arc-melted alloys with equiatomic compositions of YGdTbDyLu or GdTbDyTmLu in an Ar atmosphere from elements with a purity of 99.9 wt%. In either case, the resulting microstructure consisted of an HCP phase with undetermined minor inclusions that could be due to stacking faults. The similar crystal structure of the elements and the small atomic size difference of about 5% between Y and the heavy lanthanides have been cited as the factors promoting the formation of a single-phase HCP alloy. Zhao et al. [25]

synthesized equiatomic YLaGdTbHo alloy by arc-melting 99.9 wt% pure metals in a Ti-gettered high-purity Ar atmosphere and homogenizing the ingot by remelting it four times. The microstructure consisted of single-phase HCP with undetermined inclusions enriched in Y and O.

Youssef et al. [26] used ball milling of 99% pure metal powders in an Ar atmosphere initially at liquid-N₂ temperature and then at room temperature to prepare a low-density HEA with atomic proportions, Li₂MgAl₂Sc₂Ti₃. The as-milled microstructure was nanocrystalline FCC with a grain size of 12 nm. Upon annealing at 500 °C for 1 h, the materials transformed to HCP. This transformation did not occur when N (0.4 at.%) and O (1.4 at.%) contamination was accidentally introduced. DFT calculations showed that the HCP phase had a lower energy than the FCC phase. The occurrence of a solid solution is surprising in view of factors mentioned previously, including small atomic size difference and low heat of mixing. Many of the binary systems in this HEA are immiscible or form intermetallic phases. It is worth exploring if the nanocrystalline grain size contributes to the stability of the solid solution in this case.

Recently, thermal decomposition of 5- and 6-component salts in a hydrogen flow has been used to synthesize single-phase HCP alloys containing precious metals [20]. The alloy composition was Ru_{0.19}Rh_{0.20}Re_{0.21}Os_{0.22}Ir_{0.19}. The space group was $P6_3/mmc$ with lattice constants $a = 0.273$ nm and $c = 0.434$ nm. The material exhibited twins and planar defects. The HCP phase was found to be stable up to 1200 °C. It was also stable under hydrostatic compression to 45 GPa at room temperature. The alloy exhibited enhanced electrocatalytic activity for methanol oxidation.

Extreme processing has been shown to stabilize the HCP phase in the CrMnFeCoNi equiatomic alloy [27]. Extreme processing conditions include high temperature, high pressure, severe plastic deformation, radiation fields, and high electric or magnetic fields. This alloy is known to exist in the single-phase FCC structure from experiments at room temperature [11] and cryogenic temperatures as low as 77 K [16]. However, ab initio calculations [4] indicated that the HCP phase was stable at temperatures below 340 K. Tracy et al. [27] observed a martensitic transformation from FCC to HCP at a pressure of 14 GPa. Some of the HCP phase was retained after the release of pressure. Zhang et al. [28] observed the transformation from FCC to HCP to occur between 22 and 41 GPa, with the two-phase mixture existing over this broad pressure range. Upon return to ambient pressure, the HCP phase was stable up to a temperature of 633 K. The FCC to HCP phase transition was also observed recently by Moon et al. [29] in Cr₂₆Mn₂₀Fe₂₀Co₂₀Ni₁₄ alloy following high-pressure torsion at cryogenic temperatures. The crystal structure of this HCP phase was consistent with that of the HCP phase reported by Zhang et al.

[28]. These results demonstrate that extreme processing conditions, such as high pressure and severe plastic deformation, can be used to stabilize HCP phases or create multiphase HEAs with desirable properties.

In addition to the extremes of pressure or shear stress in the above examples, one can consider the combination of radiation and elevated temperature as an extreme processing condition appropriate for the study of phase formation under external driving forces. One of the oldest known MPEAs (MoTcRuRhPd) forms in nuclear fuel as a single-phase HCP alloy under the extreme operating conditions of a nuclear reactor. Fission product metals, such as Mo, Tc, Ru, Rh, Pd, Ag, Cd, and Te, accumulate into HCP alloy particles, known as the epsilon (ϵ) phase. About 1.7 billion years ago, fission products from natural self-sustaining nuclear reactions in a uranium deposit at Oklo in Gabon formed what could be considered the oldest MPEA known to humanity [30]. This phase has been the subject of several experimental studies long before HEAs came into vogue.

About 50 years ago, Bramman et al. [31] established that spherical ϵ -phase fission product aggregates in fuel are composed of Mo, Tc, Ru, Rh, and Pd and determined the structure to be hexagonal with lattice constants $a = 0.273$ nm and $c = 0.444$ nm. These inclusions appeared white in ceramographs and were typically less than 20 μm in diameter. The authors proposed that metallic fission products close to the high temperature center of the fuel pellet may melt and coalesce but that most of the observed inclusions accumulated through solid state diffusion of individual elements. The authors also cast an ingot of Mo 43.5 wt%, Ru 35.5 wt%, Tc 17.7 wt%, and Rh 3.3 wt% to study this MPEA in detail. The structure was mainly HCP with a second phase of Mo_5RuTc that constituted no more than 5%. This MPEA was tough, malleable, insoluble in common acids, and unaffected by exposure to normal etching reagents. Larger (700 μm) diameter particles with a similar structure but slightly different composition compared with that in the previously mentioned fission product study were extracted from irradiated fuel by O'Boyle et al. [32], who proposed the formation of these particles by migration of fission products along grain boundaries.

Kleykamp and coworkers [33, 34, 35] systematically studied the composition, structure, and thermodynamics of MPEA precipitates in uranium oxide nuclear fuels using X-ray diffraction and microanalysis. The metallic phases they observed included the HCP ϵ -phase containing Mo, Tc, Rh, and Pd; the BCC β -phase containing Mo, Tc, and Ru; and the FCC α -phase enriched in Pd, Ru, and Rh. The α -phase formed at low Mo and high Pd content. At high oxygen potential, selective oxidation of Mo resulted in the ϵ -phase transforming into a two-phase mixture of ϵ and α [36]. Furthermore, they observed a σ -phase (Mo_5Ru_3), which formed at high Mo and

low Pd content. Given the challenge of understanding the phase space as a function of temperature in a quinary diagram, Kleykamp et al. [33] developed pseudo-ternary diagrams for this system. Figure 1 shows such a diagram that includes compositions of metallic particles extracted from nuclear fuel [37], with different symbols representing different extraction processes. Not all phases, in particular, the ζ and σ phases, are labeled in this diagram for clarity.

More recent studies have focused on the nanostructure of these alloy particles. Yang et al. [38] have reviewed the radiation response and defect properties of HEAs. Cui et al. [39] have characterized MPEA particles from low burn-up fuel to determine composition and lattice constants. The composition was rich in Mo, Ru, and Pd and had the HCP structure. Buck et al. [37] have observed particles of 10–300 nm diameter with ϵ -phase (hexagonal) structure in used nuclear fuel. The particles exhibited a unique nanostructure with crystallites of 1–3 nm diameter and amorphous regions as seen in Fig. 2. Aggregates of the MPEA particles can be seen in the transmission electron microscopy image. The diffraction patterns show that the particles have the ϵ -phase HCP structure. Similar nanoparticles have also been found in specimens from the Oklo “natural reactor.” Lucuta et al. [40] have reported the formation of spherical Mo–Ru–Rh–Pd MPEA precipitates in simulated nuclear fuel.

An interesting idea was to use the ϵ -phase particle as an aggregate form that could serve to isolate and immobilize nuclear waste by-products. To this end, Crum et al. [41] have investigated spark plasma sintering, microwave sintering, and hot isostatic pressing to produce an ϵ -phase-based aggregate that could serve as a waste form to immobilize Tc and metals

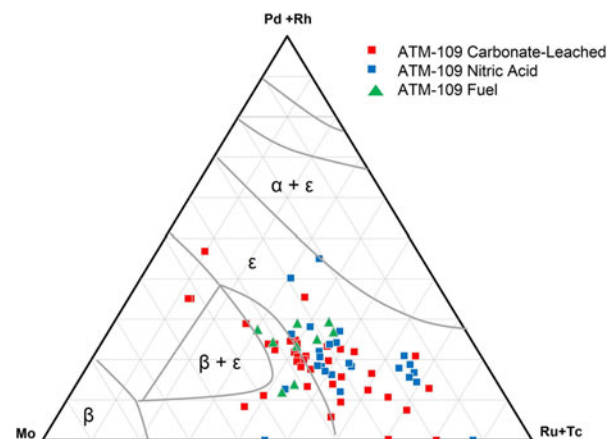


Figure 1: Compositions of MPEA particles superimposed on the pseudo-ternary phase diagram proposed by Kleykamp et al. [33]. Different symbols represent the particles in as-received nuclear fuel ATM-109 (green triangle), after nitric acid dissolution (blue square), and carbonate-peroxide dissolution processes (red square). Reprinted from Buck et al. [37] with permission from Elsevier. (color online)

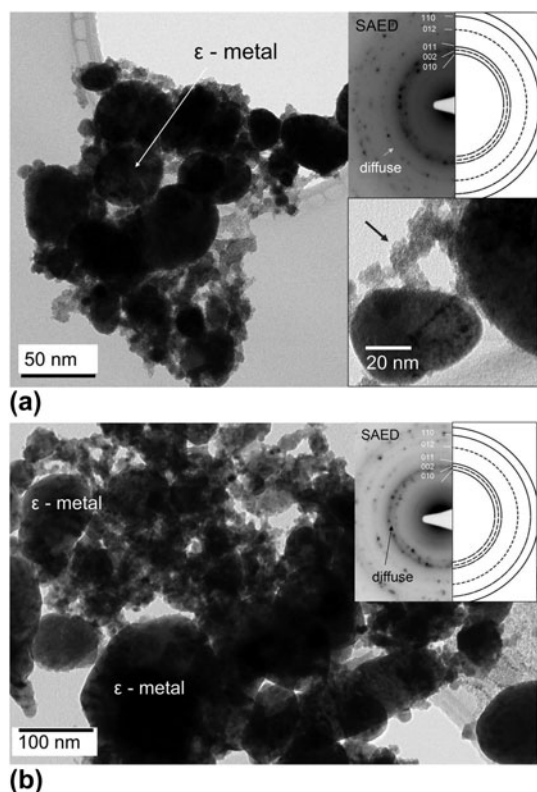


Figure 2: Bright field transmission electron microscopy image of metallic particle agglomerates from (a) carbonate-peroxide dissolved used fuel. The inset shows selected area electron diffraction (SAED) pattern and fit to ϵ -Ru HCP structure. The image in the bottom right-hand corner is a higher magnification image of the ϵ -metal particles clearly showing that some particles are isolated 1–2 nm particles and (b) nitric acid dissolved used fuel with inset SAED pattern and match to ϵ -Ru metal. Reprinted from Buck et al. [37] with permission from Elsevier.

that are part of undissolved solids in nuclear fuel processing. The resulting fission product MPEA has been observed to be chemically durable and resistant to attack by acid solutions that dissolve UO_2 fuel [31]. The study of the thermodynamics and formation process of MoTcRuRhPd HEA can help design a metallic waste form to immobilize the volatile ^{99}Tc , which has a long half-life of $\sim 211,000$ years and is usually present as soluble TcO_4^- .

Results and discussion

Figure 3 shows an HAADF-STEM micrograph of doped ceria irradiated with He^+ ions at 673 K. The micrograph is from the peak damage region irradiated to 13 displacements per atom. This implies that the average atom has been knocked out of its site 13 times. In ceria, molecular dynamics simulations [50] show that most of the atoms displaced by energetic particles return to lattice sites, leaving behind a few vacancy clusters and interstitial clusters. Such defects can play an important role in enhancing atomic diffusion. The ceria remained crystalline

rather than becoming amorphous. Small precipitates were evident in the HAADF-STEM images from atomic number (Z) contrast, and the EDS-STEM maps showed that these clusters are enriched in Pd. These enrichments/particles, with a diameter of 3 nm or less, formed after the irradiation and were not seen in the sample prior to irradiation. The clusters were found predominantly near grain boundaries and dislocations. These findings suggest that Pd is the most mobile species and it is likely to migrate along extended defects aided by point defects produced by radiation. Diffusion of metals along grain boundaries to form MPEA particles (ϵ -phase) in UO_2 was proposed initially by O'Boyle et al. [32].

Figure 4 shows an HAADF-STEM micrograph in gray of the peak damage region of a metal-doped ceria sample that was annealed after irradiation. This sample was annealed at 1373 K for 10 h in air following 90 keV He^+ irradiation at 673 K. The annealing temperature is typical of the centerline temperature of a nuclear fuel pellet in a reactor. The corresponding STEM-EDS maps are shown for O, Mo, Ru, Rh, Pd, Ag, Ce, Re, and Ir. The EDS maps include Ag, which is an impurity element that was most likely introduced unintentionally from silver paste used to mount samples for irradiation. The Ir signal could be an artifact. Following annealing, five other metals joined Pd to form areas of enrichment along defects and voids within the film. Large particles of 100 nm diameter were observed, and they were enriched in Mo, Ru, Ag, Pd, Re, and Rh. These precipitates formed throughout the ceria matrix and preferentially along grain boundaries, cracks, and dislocation lines. The extended defects could serve as rapid migration pathways for metals to join the initial Pd cluster and produce MPEA particles. These results show the effects of thermal and radiation-enhanced diffusion on the formation of MPEA nanoparticles from a uniform distribution of metal atoms under extreme processing conditions. Further details about the evolution of these particles, including results from atom probe tomography, can be found in the recent report of Jiang et al. [52]. Previous reports on ϵ -phase particles had presented only the final microstructural state of MPEA particles in irradiated fuel. This work has revealed the early stages of MPEA formation. Due to the small size of the clusters and the fact that they are embedded in a ceramic matrix, we have not been able to unambiguously determine the crystal structure.

To understand and predict phase formation in this alloy system, we have used the ASAP tool of King and McGregor [44] to calculate structure and electronic and thermodynamic properties of HCP HEAs. The compositions of experimentally reported and computationally predicted HCP HEAs and their properties are provided in Table S1 of the Supplementary material. Several of these compositions have been presented in the Supplementary material table of a recent work by Gao et al.

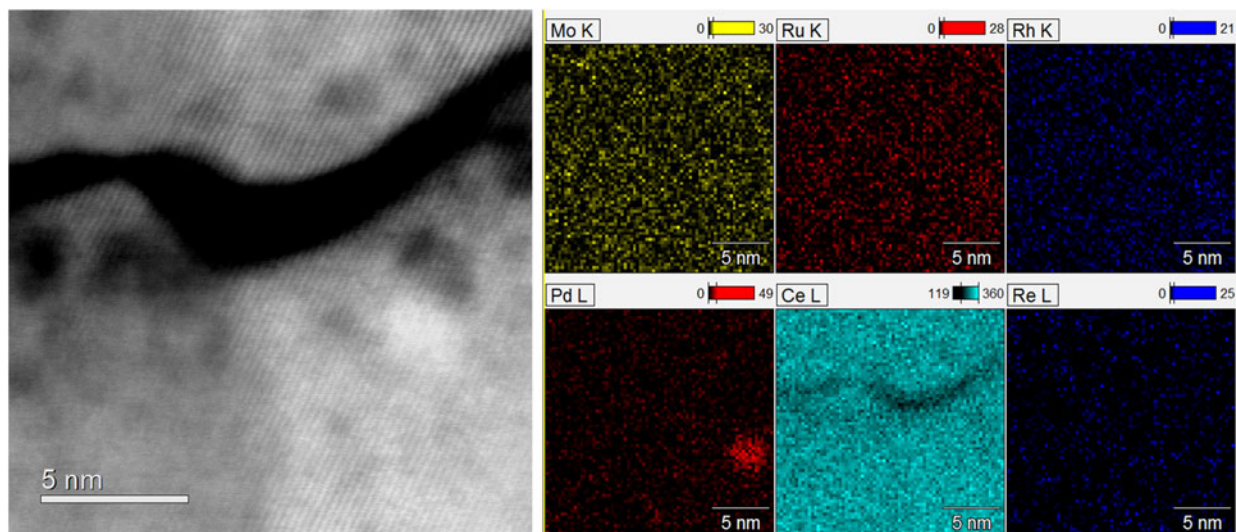


Figure 3: HAADF-STEM images from CeO₂ doped with Mo, Ru, Rh, Pd, and Re and irradiated with 90 keV He⁺ ions to a fluence of 4×10^{17} ions/cm² at 673 K, with STEM-EDS maps of Mo, Ru, Rh, Pd, Ce, and Re showing Pd nanoclusters. (color online)

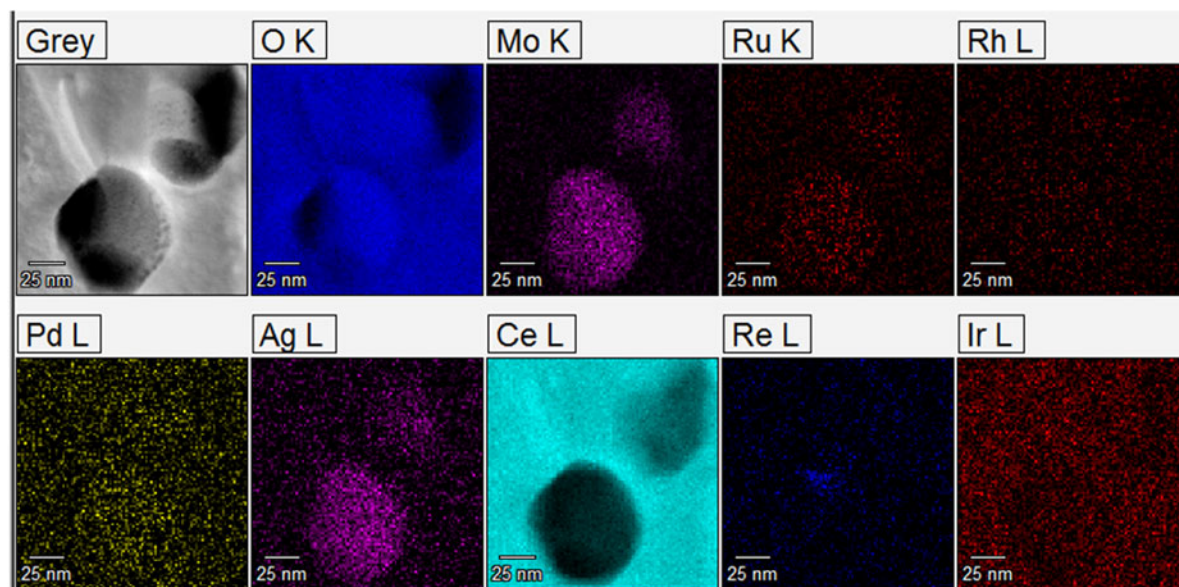


Figure 4: (a) HAADF-STEM micrograph from a CeO₂ sample doped with Mo, Ru, Rh, Pd, and Re that was annealed at 1373 K for 10 h in air after irradiation with 90 keV He⁺ ions to a fluence of 4×10^{17} ions/cm² at 673 K. (b–k) STEM-EDS maps of Ce, O, Mo, Re, Pd, Ru, Rh, and impurities Si and Ca. (color online)

[53], but the values of properties differ. Figure 5 shows the VEC of experimentally synthesized HCP HEAs as a function of the atomic size mismatch parameter δr . The alloys considered belong to the MoTcRuRhPd (ϵ -phase), ALLiMgScTi, YLaGdTb-DyHoTmLu, IrOsReRhRu, ALLiMgScTi, and CoCrFeMnNi families. It has been proposed [8] that BCC solid solutions form for VEC < 6.8 and FCC solid solutions for VEC > 8. In between these values, FCC and BCC phases were expected to coexist. Given the identical first neighbor atomic arrangements in FCC and HCP structures, it may be worthwhile to test the above criterion by substituting HCP for FCC. The ϵ -phase

HCP HEAs have a VEC between 6.8 and 8. CoCrFeMnNi has a VEC of 8 and shows a stable phase at elevated temperature. The lanthanide HEAs and Ir_{0.19}O_{0.21}Re_{0.21}Rh_{0.20}Ru_{0.19} have a VEC of 8 or higher. Al₂Li₂MgSc₂Ti₃ is an outlier in that it has a much lower VEC of 2.8 and a large atomic size mismatch δr of 4.66%. The other HCP HEAs have δr between 1 and 2.1%.

Senkov and Miracle [43] have reviewed the statistical analysis of experimental data that suggests that solid solution can exist if δr is < 6.2% and ΔH_{SS} is between -12 and 5 kJ/mol. Intermetallic phases can exist for δr > 3% and negative ΔH_{SS} , while the material is likely to be amorphous for δr > 6.2% and

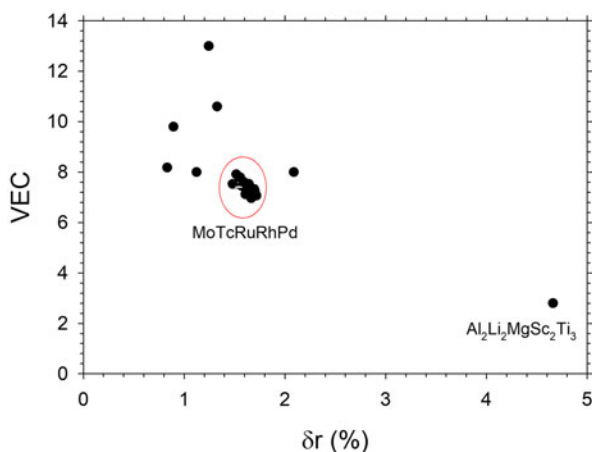


Figure 5: VEC of HCP HEAs as a function of atomic size mismatch. (color online)

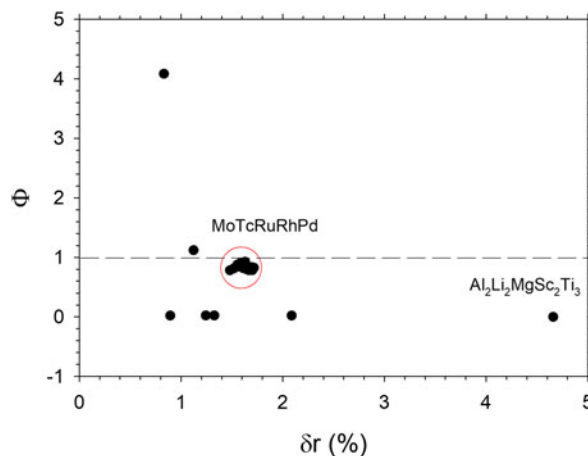


Figure 7: Φ parameter, which is a ratio of Gibbs free energy of the solid solution to that of the competing phase, for HCP HEAs as a function of atomic size mismatch. (color online)

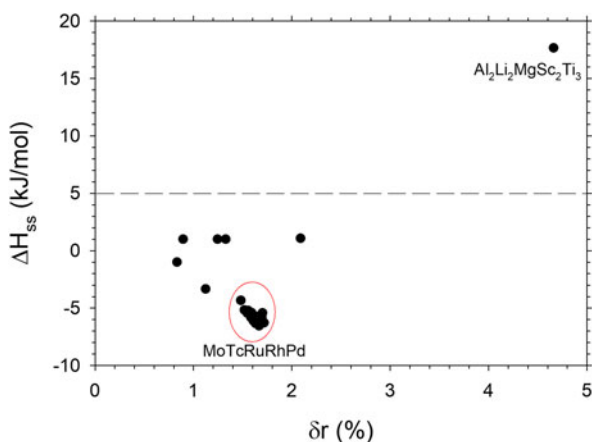


Figure 6: Enthalpy of mixing for HCP HEA solid solutions as a function of atomic size mismatch. (color online)

ΔH_{SS} between -40 and -12 kJ/mol. The value of ΔH_{SS} is plotted against δr for HCP HEAs in Fig. 6. This criterion for solid solutions holds for MoTcRuRhPd, CoCrMnFeNi, lanthanides, and $\text{Ir}_{0.19}\text{Os}_{0.21}\text{Re}_{0.21}\text{Rh}_{0.20}\text{Ru}_{0.19}$, and intermetallic compound formation is unlikely because the δr is $<3\%$. The lanthanides have a small positive ΔH_{SS} that still meets the criterion for solid solution formation. $\text{Al}_2\text{Li}_2\text{MgSc}_2\text{Ti}_3$ is an outlier in the upper right corner and does not meet any of these criteria because it has a large positive ΔH_{SS} .

Figure 7 is a plot of the parameter Φ expressed as a ratio of Gibbs free energies of competing phases as a function of the atomic size mismatch parameter. Formation of single-phase random solutions of HEA is expected for $\Phi \geq 1$ and $\delta r \leq 6.6$. Only equiatomic CoCrMnFeNi and $\text{Ir}_{0.19}\text{Os}_{0.21}\text{Re}_{0.21}\text{Rh}_{0.20}\text{Ru}_{0.19}$ are predicted to be single-phase solid solutions. Both of these are predicted to form FCC solutions. This prediction has been experimentally confirmed for both these systems over a certain temperature and composition range. The ϵ -phase alloys

(MoTcRuRhPd) come close to meeting this criterion because they have Φ values between 0.78 and 0.92 just below the threshold of 1. A recent DFT study has concluded that below about 2000 K the ϵ -phase may undergo partial ordering [55]. It is also worth considering that the ϵ -phase often occurs as a nanoparticle and nanosize effects due to the influence of surface free energy have been shown to stabilize the HCP phase of Rh [56]. The lanthanides and $\text{Li}_2\text{MgAl}_2\text{Sc}_2\text{Ti}_3$ have a Φ value close to 0. In the case of the lanthanides, the G_{\max} value in Eq. (8) is uncertain and the calculation assumes a large “worst-case scenario value” for this parameter. The $\text{Li}_2\text{MgAl}_2\text{Sc}_2\text{Ti}_3$ alloy had FCC structure as-milled but transformed into HCP after annealing at 500 °C for 1 h and the grain size was estimated to be 26 nm. This alloy was synthesized under nonequilibrium conditions. The annealing temperature is too low and annealing time too short to equilibrate this material. It is likely that the HCP phase is metastable and a multiphase microstructure could form upon prolonged annealing at elevated temperature. Calculations of phase stability are limited by gaps in thermodynamic data for the alloys of interest. The experimentally characterized phases may be metastable and influenced by size effects. More rigorous studies are needed to identify the stable phases and assess the reliability of the Φ parameter for the prediction of HCP HEAs.

The Ω parameter that considers the ratio of the entropy of mixing and enthalpy of mixing has also been used to predict the occurrence of solid solutions. According to Yang and Zhang, solid solutions form in HEAs for values of $\Omega \geq 1.1$ and $\delta r \leq 6.6\%$. An intermetallic phase or amorphous material is expected to result for smaller Ω and larger δr . Figure 8 is a plot of Ω as a function of δr . $\text{Li}_2\text{MgAl}_2\text{Sc}_2\text{Ti}_3$ fails to meet this criterion with an Ω value of 0.96 but the δr

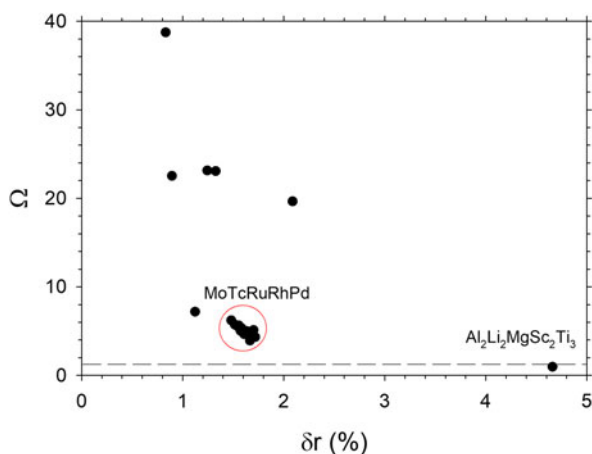


Figure 8: The ratio of entropic and enthalpic contributions to the free energy of mixing, Ω , as a function of atomic size mismatch for HCP HEAs. (color online)

value is within the specified range. All other HCP alloys plotted meet this criterion. However, Youssef et al. [26] have calculated the Ω value to be 42.6, which meets this criterion. The discrepancy between the two values of Ω probably stems from differences in the estimates of ΔH_{SS} and points to the need for obtaining reliable thermodynamic data and establishing data standards. As discussed above, the observed HCP structure of $\text{Li}_2\text{MgAl}_2\text{Sc}_2\text{Ti}_3$ may not be the stable phase, given that the alloy is an outlier compared to the other HCP HEAs studied here.

One must exercise caution in using these thermodynamic parameters to predict single-phase solid solutions. The enthalpies calculated using Miedema's model [45] correspond to liquid binary alloys. Moreover, the factor of 4 in Eq. (3) is appropriate for binary alloys. A different factor may be appropriate for MPEAs. Of the different criteria considered, the Ω parameter appears to be the most appropriate for predicting the stability of HCP HEAs and the Φ parameter is also promising. The above analysis has been extended to a list of HCP HEAs computationally predicted by Gao et al. [21] using CALPHAD and phase diagram inspection, and the results are shown in Table S1 of the Supplementary material. Many of these alloys appear to be stable as solid solutions based on Ω and δr . Several of these alloys are predicted to form single-phase solid solution based on the Φ parameter. While these parameters provide a thermodynamic basis for alloy design, the cost of alloys listed in the Supplementary material is a practical consideration for alloy selection. The HCP alloy compositions listed are one to two orders of magnitude more expensive than Fe-based (FCC or BCC) HEAs, for instance, CoCrFeMnNi. The high cost makes these HCP HEAs better suited for applications such as catalysis or nuclear waste immobilization instead of structural applications.

Previous work has identified the HCP ϵ -phase as a promising waste form for the immobilization of Tc separated from nuclear waste streams or removed from off-gas [57]. The advantages of this alloy are low overall volume of waste produced, the availability of data on the alloy stability for different compositions, and the durability of natural analogs [28]. In the case of nuclear fuel dissolved in a reprocessing plant, the ϵ -metal particles and other undissolved solids, including oxides, are left behind. These HEA particles and oxides can be consolidated as a waste form. Crum et al. [41] have synthesized a model of such a waste form that contained 5 metals, Mo, Ru, Rh, Pd, and Re (surrogate for Tc), and ZrO_2 to represent undissolved oxides. The ZrO_2 concentration varied from 0 to 35 wt%. Spark plasma sintering or hot isostatic pressing was used to consolidate the samples into high-strength solids with up to 98–100% of theoretical density. The findings may change if Tc is introduced instead of Re. However, Tc melts at a much lower temperature than Re and may get incorporated into the waste form better. These results of Crum et al. [41] show that HCP HEAs can be mixed with an oxide to produce a durable cermet waste form. The present work has provided insights into the early stages of ϵ -phase formation under extreme processing conditions and the stability of HCP HEAs.

Conclusions

We have extensively reviewed and summarized the current understanding of HCP HEAs. We have characterized the early stages of HCP HEA formation in a nuclear fuel surrogate, CeO_2 , doped with Mo, Ru, Rh, Pd, and Re, irradiated with energetic He^+ ions at 673 K, and subsequently annealed at up to 1373 K for 10 h in air. Cracks and grain boundaries provide pathways for rapid diffusion of Pd initially and other metals subsequently to form alloy clusters that are likely precursors for HEA particles. Radiation-enhanced diffusion plays an important role at 673 K in the initial stages of nanoparticle formation from a uniform dispersion of the individual metals. Thermal diffusion contributes to alloying and particle coarsening. This extreme environment creates a set of conditions in nuclear fuel that drive the formation of stable alloy particles with HCP structure. We have examined the properties of different HCP compositions in the MoTcRuRhPd system reported in the literature and found that single-phase solid solutions are thermodynamically stable over a broad range of composition based on the Ω parameter that considers the ratio of entropic and enthalpic terms. This alloy system may be a viable waste form for the immobilization of long-lived ^{99}Tc , considering the reported chemical durability of the alloy. The thermodynamic analysis was extended to all known HCP HEAs. These alloys satisfy solid solution stability criteria based on VEC, atomic size

mismatch, enthalpy of mixing, and the Ω parameter, except for $\text{Al}_2\text{Li}_2\text{MgSc}_2\text{Ti}_3$, an outlier for which the HCP phase may be metastable.

AU4 Details of experiments and calculations

We irradiated and annealed ceria doped with Mo, Ru, Rh, Pd, and Re to examine the early stages of ϵ -phase MPEA formation under the extreme processing conditions of a nuclear reactor fuel without the radiological concerns associated with irradiating nuclear fuel in a reactor. CeO_2 is a known surrogate for UO_2 with the same cubic fluorite crystal structure. Re served as a substitute for Tc, and the individual dopant weight percents were based on typical metal inventory in the ϵ -phase found in irradiated fuel. We used pulsed laser deposition in 10^{-2} torr Ar atmosphere from a target with composition 95 wt% CeO_2 , 2 wt% Mo, 1.5 wt% Ru, 0.25 wt% Rh, 0.75 wt% Pd, and 0.5 wt% Re to grow the doped ceramic on polycrystalline yttria-stabilized zirconia substrates. The substrate temperature was held at 823 K during growth. The energy density of the pulsed KrF excimer laser operating at 5 Hz was 2.4 J/cm^2 . The average growth rate of the uniformly doped CeO_2 film was 0.2 nm/s . We then irradiated the film with normally incident 90 keV He^+ ions at 673 K to a fluence up to $4 \times 10^{17} \text{ ions/cm}^2$ and used beam rastering to cover a $10 \times 10\text{-mm}$ area. At this fluence, the estimated peak displacement dose at a depth of 324 nm was 13 displacements per atom and the peak He concentration at a depth of 372 nm was 23 at.%. We annealed some of the irradiated samples and unirradiated samples in air at 1073 K or 1373 K for 10 h to study thermal effects in addition to radiation effects driving the MPEA particle formation.

We prepared cross-sectional transmission electron microscopy specimens using a beam-focused ion beam-integrated scanning electron microscope. We used high-angle annular dark field scanning transmission electron microscopy (HAADF-STEM) with an aberration-corrected JEM ARM 200CF microscope equipped with a cold field emitter and performed energy dispersive spectroscopy (EDS) using a Gatan Quantum 965 spectrometer with a proprietary JEOL Centurio Si-drift EDS detector. We performed STEM-EDS elemental mapping from selected areas with a voltage of 200 kV or 80 kV. These characterization techniques are well-suited to study nanoparticles dispersed in a ceramic matrix. As shown in Fig. S1 of the Supplementary material, phenomena occurring under extreme processing conditions of irradiation and high temperature drive the formation of sparsely distributed HCP particles, typically micrometer in size, in the UO_2 matrix. The ceramic CeO_2 used in this work serves as a nonradioactive surrogate for UO_2 .

We calculated the thermodynamic properties [43] of HCP HEAs reported in the literature and predicted by calculations

using the Alloy Search and Predict (ASAP) tool developed by King and McGregor [44]. The parameters calculated are listed below.

δr quantifies the atomic size difference of the HEA made of N metals i with atomic fraction c_i and atomic radius r_i as shown below.

$$\delta r = 100 \times \sqrt{\sum_{i=1}^N c_i \left(1 - \frac{r_i}{\bar{r}}\right)^2} \quad , \quad (1)$$

$$\bar{r} = \sum_{i=1}^N c_i r_i \quad . \quad (2)$$

The enthalpy of mixing of the solid solution is based on the enthalpy of mixing per mole H_{ij} of pairs of metals i and j as follows:

$$\Delta H_{SS} = \sum_{i=1}^N \sum_{j>i} 4H_{ij}c_i c_j \quad , \quad (3)$$

H_{ij} was determined from Miedema's model [45] applied to a liquid binary alloy. The configurational entropy of mixing of the solid solution is given by the following equation:

$$\Delta S_{SS} = -R \sum_{i=1}^N c_i \ln(c_i) \quad . \quad (4)$$

Here, R is the universal gas constant [$8.314 \text{ J}/(\text{mol K})$].

To understand phase stability, we must account for both enthalpy and entropy by considering the Gibbs free energy change ΔG .

$$\Delta G_{SS} = \Delta H_{SS} - T\Delta S_{SS} \quad , \quad (5)$$

where ΔG_{SS} is the change in Gibbs free energy for forming a disordered solid solution at temperature T starting with individual elements. Yang and Zhang [46] have proposed a criterion based on an omega parameter for predicting solid solution formation in HEAs by comparing the relative importance of enthalpic and entropic contributions shown in Eqs. (3) and (4), respectively.

$$\Omega = \frac{T_m^{\text{HEA}} \Delta S_{SS}}{|\Delta H_{SS}|} \quad . \quad (6)$$

The HEA melting temperature (T_m^{HEA}) is obtained from the melting temperature of each element i (T_m^i) using the rule of mixtures.

$$T_m^{\text{HEA}} = \sum_{i=1}^N c_i T_m^i \quad . \quad (7)$$

Criteria for solid solution stability based on the relative values of Gibbs free energy change for competing solid solution

and intermetallic phases have also been proposed in the literature [43]. King et al. [47] have proposed a parameter Φ based on the ratio of these Gibbs free energy values:

$$\Phi = \frac{-\Delta G_{SS}}{|\Delta G_{max}|} \quad (8)$$

Here, ΔG_{max} was defined as the lowest Gibbs free energy change on forming an intermetallic or the highest Gibbs free energy change for segregation when the individual elements are mixed. Troparevsky et al. [48] have used high-throughput DFT calculations to develop a database of enthalpies of formation of binary intermetallic compounds and specified an optimal range of values at which a solid solution is likely to form. Finally, for the sake of completeness, we have also calculated the valence electron concentration (VEC) of alloys obtained as a weighted average of VEC of individual metals. Massalski [49] has defined the VEC to include all the electrons in the valence band, including the d-electrons.

$$VEC_{HEA} = \sum_{i=1}^N c_i VEC_i \quad (9)$$

Acknowledgments

The authors thank D.J.M. King for thoughtful suggestions about the thermodynamics of MPEAs. This work was supported by the Nuclear Process Science Initiative (NPSI) under the Laboratory Directed Research and Development (LDRD) Program at the Pacific Northwest National Laboratory, a multi-program national laboratory operated by Battelle for the U.S. Department of Energy under Contract DE-AC05-76RL01830. Ion irradiation was performed at Texas A&M University.

Supplementary material

To view supplementary material for this article, please visit <https://doi.org/10.1557/jmr.2018.438>.

References

1. J.W. Yeh, S.K. Chen, S.J. Lin, J.Y. Gan, T.S. Chin, T.T. Shun, C.H. Tsau, and S.Y. Chang: Nanostructured high-entropy alloys with multiple principal elements: Novel alloy design concepts and outcomes. *Adv. Eng. Mater.* **6**, 299 (2004).
2. B. Cantor, I. Chang, P. Knight, and A. Vincent: Microstructural development in equiatomic multicomponent alloys. *Mater. Sci. Eng., A* **375**, 213 (2004).
3. L.J. Santodonato, Y. Zhang, M. Feygenson, C.M. Parish, M.C. Gao, R.J. Weber, J.C. Neufeld, Z. Tang, and P.K. Liaw: Deviation from high-entropy configurations in the atomic distributions of a multi-principal-element alloy. *Nat. Commun.* **6**, 5964 (2015).
4. D. Ma, B. Grabowski, F. Körmann, J. Neugebauer, and D. Raabe: Ab initio thermodynamics of the CoCrFeMnNi high entropy alloy: Importance of entropy contributions beyond the configurational one. *Acta Mater.* **100**, 90 (2015).
5. A. Melnick and V. Soolshenko: Thermodynamic design of high-entropy refractory alloys. *J. Alloys Compd.* **694**, 223 (2017).
6. D. Miracle and O. Senkov: A critical review of high entropy alloys and related concepts. *Acta Mater.* **122**, 448 (2017).
7. M. Widom: Modeling the structure and thermodynamics of high-entropy alloys. *J. Mater. Res.* **1** (2018).
8. Y. Zhang, T.T. Zuo, Z. Tang, M.C. Gao, K.A. Dahmen, P.K. Liaw, and Z.P. Lu: Microstructures and properties of high-entropy alloys. *Prog. Mater. Sci.* **61**, 1 (2014).
9. C.G. Schön, T. Duong, Y. Wang, and R. Arróyave: Probing the entropy hypothesis in highly concentrated alloys. *Acta Mater.* **148**, 263 (2018).
10. E. Pickering and N.G. Jones: High-entropy alloys: A critical assessment of their founding principles and future prospects. *Int. Mater. Rev.* **61**, 183 (2016).
11. F. Otto, A. Dlouhý, C. Somsen, H. Bei, G. Eggeler, and E.P. George: The influences of temperature and microstructure on the tensile properties of a CoCrFeMnNi high-entropy alloy. *Acta Mater.* **61**, 5743 (2013).
12. S. Middleburgh, D. King, and G. Lumpkin: Atomic scale modelling of hexagonal structured metallic fission product alloys. *R. Soc. Open Sci.* **2**, 140292 (2015).
13. M.C. Gao, C. Zhang, P. Gao, F. Zhang, L. Ouyang, M. Widom, and J. Hawk: Thermodynamics of concentrated solid solution alloys. *Curr. Opin. Solid State Mater. Sci.* **21**, 238–251 (2017). AU6
14. O. Senkov, J. Miller, D. Miracle, and C. Woodward: Accelerated exploration of multi-principal element alloys with solid solution phases. *Nat. Commun.* **6**, 6529 (2015).
15. S. Gorsse, D.B. Miracle, and O.N. Senkov: Mapping the world of complex concentrated alloys. *Acta Mater.* **135**, 177 (2017).
16. B. Gludovatz, A. Hohenwarter, D. Catoor, E.H. Chang, E. P. George, and R.O. Ritchie: A fracture-resistant high-entropy alloy for cryogenic applications. *Science* **345**, 1153 (2014).
17. Z. Tang, L. Huang, W. He, and P.K. Liaw: Alloying and processing effects on the aqueous corrosion behavior of high-entropy alloys. *Entropy* **16**, 895 (2014).
18. M-H. Chuang, M-H. Tsai, W-R. Wang, S-J. Lin, and J-W. Yeh: Microstructure and wear behavior of $Al_xCo_{1.5}CrFeNi_{1.5}Ti_y$ high-entropy alloys. *Acta Mater.* **59**, 6308 (2011).
19. M.A. Hemphill, T. Yuan, G. Wang, J. Yeh, C. Tsai, A. Chuang, and P. Liaw: Fatigue behavior of $Al_{0.5}CoCrCuFeNi$ high entropy alloys. *Acta Mater.* **60**, 5723 (2012).
20. K.V. Yussenko, S. Riva, P.A. Carvalho, M.V. Yussenko, S. Arnaboldi, A.S. Sukhikh, M. Hanfland, and S.A. Gromilov: First hexagonal close packed high-entropy alloy with outstanding

- stability under extreme conditions and electrocatalytic activity for methanol oxidation. *Scr. Mater.* **138**, 22 (2017).
21. **M.C. Gao, B. Zhang, S. Guo, J. Qiao, and J. Hawk:** High-entropy alloys in hexagonal close-packed structure. *Metall. Mater. Trans. A* **47**, 3322 (2016).
 22. **M. Feuerbacher, M. Heidelmann, and C. Thomas:** Hexagonal high-entropy alloys. *Mater. Res. Lett.* **3**, 1 (2015).
 23. **M.C. Gao and D.E. Alman:** Searching for next single-phase high-entropy alloy compositions. *Entropy* **15**, 4504 (2013).
 24. **A. Takeuchi, K. Amiya, T. Wada, K. Yubuta, and W. Zhang:** High-entropy alloys with a hexagonal close-packed structure designed by equi-atomic alloy strategy and binary phase diagrams. *JOM* **66**, 1984 (2014).
 25. **Y. Zhao, J. Qiao, S. Ma, M. Gao, H. Yang, M. Chen, and Y. Zhang:** A hexagonal close-packed high-entropy alloy: The effect of entropy. *Mater. Des.* **96**, 10 (2016).
 26. **K.M. Youssef, A.J. Zaddach, C. Niu, D.L. Irving, and C.C. Koch:** A novel low-density, high-hardness, high-entropy alloy with close-packed single-phase nanocrystalline structures. *Mater. Res. Lett.* **3**, 95 (2015).
 27. **C.L. Tracy, S. Park, D.R. Rittman, S.J. Zinkle, H. Bei, M. Lang, R.C. Ewing, and W.L. Mao:** High pressure synthesis of a hexagonal close-packed phase of the high-entropy alloy CrMnFeCoNi. *Nat. Commun.* **8**, 15634 (2017).
 28. **F. Zhang, Y. Wu, H. Lou, Z. Zeng, V.B. Prakapenka, E. Greenberg, Y. Ren, J. Yan, J.S. Okasinski, X. Liu, Y. Liu, Q. Zeng, and Z. Lu:** Polymorphism in a high-entropy alloy. *Nat. Commun.* **8**, 15687 (2017).
 29. **J. Moon, Y. Qi, E. Tabachnikova, Y. Estrin, W-M. Choi, S-H. Joo, B-J. Lee, A. Podolskiy, M. Tikhonovsky, and H.S. Kim:** Microstructure and mechanical properties of high-entropy alloy Co₂₀Cr₂₆Fe₂₀Mn₂₀Ni₁₄ processed by high-pressure torsion at 77 K and 300 K. *Sci. Rep.* **8**, 11074 (2018).
 30. **S. Utsunomiya and R.C. Ewing:** The fate of the epsilon phase (Mo–Ru–Pd–Tc–Rh) in the UO₂ of the Oklo natural fission reactors. *Radiochim. Acta* **94**, 749 (2006).
 31. **J. Bramman, R. Sharpe, D. Thom, and G. Yates:** Metallic fission-product inclusions in irradiated oxide fuels. *J. Nucl. Mater.* **25**, 201 (1968).
 32. **D. O'Boyle, F. Brown, and A. Dwight:** Analysis of fission product ingots formed in uranium-plutonium oxide irradiated in EBR-II. *J. Nucl. Mater.* **35**, 257 (1970).
 33. **H. Kleykamp:** The chemical state of the fission products in oxide fuels. *J. Nucl. Mater.* **131**, 221 (1985).
 34. **H. Kleykamp, J. Paschoal, R. Pejsa, and F. Thümmeler:** Composition and structure of fission product precipitates in irradiated oxide fuels: Correlation with phase studies in the Mo–Ru–Rh–Pd and BaO–UO₂–ZrO₂–MoO₂ systems. *J. Nucl. Mater.* **130**, 426 (1985).
 35. **H. Kleykamp:** Constitution and thermodynamics of the Mo–Ru, Mo–Pd, Ru–Pd, and Mo–Ru–Pd systems. *J. Nucl. Mater.* **167**, 49 (1989).
 36. **K. Naito, T. Tsuji, T. Matsui, and A. Date:** Chemical state, phases and vapor pressures of fission-produced noble metals in oxide fuel. *J. Nucl. Mater.* **154**, 3 (1988).
 37. **E.C. Buck, E.J. Mausolf, B.K. McNamara, C.Z. Soderquist, and J.M. Schwantes:** Nanostructure of metallic particles in light water reactor used nuclear fuel. *J. Nucl. Mater.* **461**, 236 (2015).
 38. **T. Yang, C. Li, S.J. Zinkle, S. Zhao, H. Bei, and Y. Zhang:** Irradiation responses and defect behavior of single-phase concentrated solid solution alloys. *J. Mater. Res.* **33**, 3077 (2018).
 39. **D. Cui, V.V. Rondinella, J.A. Fortner, A.J. Kropf, L. Eriksson, D.J. Wronkiewicz, and K. Spahi:** Characterization of alloy particles extracted from spent nuclear fuel. *J. Nucl. Mater.* **420**, 328 (2012).
 40. **P.G. Lucuta, R.A. Verrall, H. Matzke, and B.J. Palmer:** Microstructural features of SIMFUEL—Simulated high-burnup UO₂-based nuclear fuel. *J. Nucl. Mater.* **178**, 48 (1991).
 41. **J.V. Crum, D. Strachan, A. Rohatgi, and M. Zumbhoff:** Epsilon metal waste form for immobilization of noble metals from used nuclear fuel. *J. Nucl. Mater.* **441**, 103 (2013).
 42. **D. Cui, J. Low, C.J. Sjoestedt, and K. Spahi:** On Mo–Ru–Tc–Pd–Rh–Te alloy particles extracted from spent fuel and their leaching behavior under Ar and H₂ atmospheres. *Radiochim. Acta* **92**, 551 (2004).
 43. **O. Senkov and D. Miracle:** A new thermodynamic parameter to predict formation of solid solution or intermetallic phases in high entropy alloys. *J. Alloys Compd.* **658**, 603 (2016).
 44. **D.J.M. King and A.J. McGregor:** *Alloy Search and Predict* (2015). Available at: <http://www.alloyasap.com>. AU7
 45. **A. Takeuchi and A. Inoue:** Classification of bulk metallic glasses by atomic size difference, heat of mixing and period of constituent elements and its application to characterization of the main alloying element. *Mater. Trans.* **46**, 2817 (2005).
 46. **X. Yang and Y. Zhang:** Prediction of high-entropy stabilized solid-solution in multi-component alloys. *Mater. Chem. Phys.* **132**, 233 (2012).
 47. **D. King, S. Middleburgh, A. McGregor, and M. Cortie:** Predicting the formation and stability of single phase high-entropy alloys. *Acta Mater.* **104**, 172 (2016).
 48. **M.C. Tropicovsky, J.R. Morris, P.R. Kent, A.R. Lupini, and G.M. Stocks:** Criteria for predicting the formation of single-phase high-entropy alloys. *Phys. Rev. X* **5**, 011041 (2015).
 49. **T.B. Massalski:** Comments concerning some features of phase diagrams and phase transformations. *Mater. Trans.* **51**, 583 (2010).
 50. **C.A. Yablinsky, R. Devanathan, J. Pakarinen, J. Gan, D. Severin, C. Trautmann, and T.R. Allen:** Characterization of swift heavy ion irradiation damage in ceria. *J. Mater. Res.* **30**, 1473 (2015).
 51. **R. Devanathan:** Molecular dynamics simulation of fission fragment damage in nuclear fuel and surrogate material. *MRS Adv.* **2**, 1225 (2017).
 52. **W. Jiang, M.A. Conroy, K. Kruska, N.R. Overman, T.C. Droubay, J. Gigax, L. Shao, and R. Devanathan:** Nanoparticle

- 1 precipitation in irradiated and annealed ceria doped with metals for
2 emulsion of spent fuels. *J. Phys. Chem. C* **121**, 22465 (2017).
- 3 **53. M.C. Gao, P. Gao, J.A. Hawk, L. Ouyang, D.E. Alman, and**
4 **M. Widom:** Computational modeling of high-entropy alloys:
5 Structures, thermodynamics and elasticity. *J. Mater. Res.* **32**, 3627
6 (2017).
- 7 **54. S. Guo, C. Ng, J. Lu, and C. Liu:** Effect of valence electron
8 concentration on stability of fcc or bcc phase in high entropy
9 alloys. *J. Appl. Phys.* **109**, 103505 (2011).
- 10
- 11
- 12
- 13
- 14
- 15
- 16
- 17
- 18
- 19
- 20
- 21
- 22
- 23
- 24
- 25
- 26
- 27
- 28
- 29
- 30
- 31
- 32
- 33
- 34
- 35
- 36
- 37
- 38
- 39
- 40
- 41
- 42
- 43
- 44
- 45
- 46
- 47
- 48
- 49
- 50
- 51
- 52
- 53
- 54
- 55
- 56
- 57
- 58
- 59
- 60
- 55. D.J.M. King, P.A. Burr, E.G. Obbard, and S.C. Middleburgh:**
DFT study of the hexagonal high-entropy alloy fission product
system. *J. Nucl. Mater.* **488**, 70 (2017).
- 56. J.L. Huang, Z. Li, H.H. Duan, Z.Y. Cheng, Y.D. Li, J. Zhu, and**
R. Yu: Formation of hexagonal-close packed (HCP) rhodium as
a size effect. *J. Am. Chem. Soc.* **139**, 575 (2017).
- 57. R.J. Serne, J.V. Crum, B.J. Riley, and T.G. Levitskaia:** *Options for*
the Separation and Immobilization of Technetium, PNNL-25834
(Pacific Northwest National laboratory, Richland, WA, 2016).

AUTHOR QUERY – jmr.2018.438

- 1 Please check the edits made to the sentence “About 1.7 billion years. . .”.
- 2 Two different versions of the figure captions were provided and so the captions that were supplied with the manuscript have been used. Please check that these are correct.
- 3 The caption to Fig. 4 refers to part (a–k) but the image as supplied does not contain a part labelled (a–k). Would you like to modify the caption or resupply the artwork?
- 4 Per new JMR editorial guidelines, the Experiments/Experimental Section now is the final section, following the Conclusion. Please confirm the change and adjust any language in this section if necessary.
- 5 Please provide the manufacturer details (company name, city/state if produced in the US or city/country name if produced outside US) for ‘JEM ARM 200CF, Gatan Quantum 965, and JEOL Centurio Si-drift EDS detector’.
- 6 Please check whether the edits made to the reference ‘13’ is correct.
- 7 Please provide the publisher name and location for reference ‘44’.

EDITOR QUERY – jmr.2018.438

There are no editor queries for this article.